Adaptive optics retinal scanner for one-micrometer light source

Kazuhiro Kurokawa*, Daiki Tamada, Shuichi Makita, and Yoshiaki Yasuno

Computational Optics Group in the University of Tsukuba, Tsukbua, Ibaraki, Japan

yasuno@optlab2.bk.tsukuba.ac.jp

Abstract: We developed an adaptive optics (AO) retinal scanner by using a light source with a center wavelength of 1-μm. In a recent study on optical coherence tomography (OCT), it was proved that 1-μm light provided higher image contrast of deep region of the eye than 840-nm light. Further, high lateral resolution retinal images were obtained with AO. In this study, we performed measurements on two normal subjects in the AO-SLO mode and analyzed its performance toward developing the AO-OCT. With AO correction, we found that the residual RMS wavefront error of ocular aberration was less than 0.1 μm. We also found that the AO retinal scanner in the AO-SLO mode enabled enhanced observation of photoreceptor mosaic.

OCIS codes: (170.4460) Ophthalmic optics and devices; (110.1080) Active or adaptive optics; (180.5810) Scanning microscopy; (170.1790) Confocal microscopy;

References and links

1. J. Liang, D. R. Williams, and D. T. Miller, "Supernormal vision and high-resolution retinal imaging through adaptive optics," J. Opt. Soc. Am. A **14**, 2884–2892 (1997).
2. A. Roorda, F. Romero-Borja, W. Donnelly, III, H. Queener, T. J. Hebert, and M. C. W. Campbell, "Adaptive optics scanning laser ophthalmoscopy," Opt. Express **10**, 405–412 (2002).
3. S. A. Burns, R. Tumber, A. E. Elsner, D. Ferguson, and D. X. Hammer, "Large-field-of-view, modular, stabilized, adaptive-optics-based scanning laser ophthalmoscope," J. Opt. Soc. Am. A **24**, 1313–1326 (2007).
4. D. C. Chen, S. M. Jones, D. A. Silva, and S. S. Oliver, "High-resolution adaptive optics scanning laser ophthalmoscope with dual deformable mirror," J. Opt. Soc. Am. A **24**, 1305–1312 (2007).
5. M. Pircher, R. J. Zawadzki, J. W. Evans, J. S. Werner, and C. K. Hitzenberger, "Simultaneous imaging of human cone mosaic with adaptive optics enhanced scanning laser ophthalmoscopy and high-speed transversal scanning optical coherence tomography," Opt. Lett. **33**, 22–24 (2008).
6. R. H. Webb, G. W. Hughes, and F. C. Delori, "Confocal scanning laser ophthalmoscope," Appl. Opt. **26**, 1492–1499 (1987).
7. D. X. Hammer, R. D. Ferguson, C. E. Bigelow, N. V. Iftimia, T. E. Ustun, and S. A. Burns, "Adaptive optics scanning laser ophthalmoscope for stabilized retinal imaging," Opt. Express **14**, 3354–3367 (2006).
8. B. Hermann, E. J. Fernandez, A. Unterhuder, A. F. Fercher, W. Drexler, P. M. Prieto, and P. Artal, " Adaptive-optics ultrahigh-resolution optical coherence tomography," Opt. Lett. **29**, 2142–2144 (2004).
9. R. J. Zawadzki, B. Cense, Y. Zhang, S. S. Choi, D. T. Miller, and J. S. Werner, "Ultrahigh-resolution optical coherence tomography with monochromatic and chromatic aberration correction," Opt. Express **16**, 8126–8143 (2008).
10. E. J. Fernández, B. Hermann, B. Považay, A. Unterhuber, H. Sattmann, B. Hofer, P. K. Ahnelt, and W. Drexler, "Ultrahigh-resolution optical coherence tomography and pancorrection for cellular imaging of the living human retina," Opt. Express **16**, 11083–11094 (2008).
11. B. Považay, B. Hofer, C. Torti, B. Hermann, A. R. Tumlinson, M. Esmaeelpour, C. A. Egan, A. C. Bird, and W. Drexler, "Impact of enhanced resolution, speed and penetration on three-dimensional retinal optical coherence tomography," Opt. Express **17**, 4134–4150 (2009).

#119325 - $15.00 USD Received 2 Nov 2009; revised 5 Jan 2010; accepted 7 Jan 2010; published 12 Jan 2010

12. Y. Wang, J. Nelson, Z. Chen, B. Reiser, R. Chuck, and R. Windeler, "Optimal wavelength for ultrahigh-resolution optical coherence tomography," Opt. Express **11**, 1411–1417 (2003).
13. A. Unterhuber, B. Považay, B. Hermann, H. Sattmann, A. Chavez-Pirson, and W. Drexler, "In vivo retinal optical coherence tomography at 1040 nm enhanced penetration into the choroid," Opt. Express **13**, 3252–3258 (2005).
14. Y. Yasuno, Y. Hong, S. Makita, M. Yamanari, M. Akiba, M. Miura, and T. Yatagai, "In vivo high-contrast imaging of deep posterior eye by 1-μm swept source optical coherence tomography and scattering optical coherence angiography," Opt. Express **15**, 6121–6139 (2007).
15. B. Považay, B. Hermann, A. Unterhuber, B. Hofer, H. Sattmann, F. Zeiler, J. E. Morgan, C. Falkner-Radler, C. Glittenberg, S. Blinder, and Wolfgang Drexler, "3D optical coherence tomography at 1050 nm versus 800 nm in retinal pathologies: enhanced performance and choroidal penetration in cataract patients," J. Biomed. Opt. **12**, 041211 (2007).
16. S. Makita, T. Fabritius, and Y. Yasuno, "Full-range, high-speed, high-resolution 1-μm spectral-domain optical coherence tomography using BM-scan for volumetric imaging of the human posterior eye," Opt. Express **16**, 8406–8420 (2008).
17. D. M. de Bruin, D. Burnes, J. Loewenstein, Y. Chen, S. Chang, T. Chen, D. Esmaili, and J. F. de Boer, "In-vivo three-dimensional imaging of neovascular age related macular degeneration using optical frequency domain imaging at 1050 nm," Invest. Ophthalmol. Vis. Sci. 07–1553 (2008).
18. Y. Yasuno, M. Miura, K. Kawana, S. Makita, M. Sato, F. Okamoto, M. Yamanari, T. Iwasaki, T. Yatagai, and T. Oshika, "Visualization of sub-retinal pigment epithelium morphologies of exudative macular diseases by high-penetration optical coherence tomography," Invest. Ophthalmol. Vis. Sci. **50**, 405–413 (2009).
19. B. Považay, B. Hermann, B. Hofer, V. Kajić, E. Simpson, T. Bridgford, and W. Drexler, "Wide-field optical coherence tomography of the choroid in vivo," Invest. Ophthalmol. Vis. Sci. **50**, 1856–1863 (2009).
20. F. C. Delori and K. P. Pflibsen, "Spectral reflectance of the human ocular fundus," App. Opt. **28**, 1061–1077 (1989).
21. M. Hammer, A. Roggan, D. Schweitzer, and G. Muller, "Optical properties of ocular fundus tissues–an in vitro study using the double-integrating-sphere technique and inverse Monte Carlo simulation," Phys. Med. Biol. **40**, 963–978 (1995).
22. A. E. Elsner, S. A. Burns, J. J. Weiter and F. C. Delori, "Infrared imaging of sub-retinal structures in the human ocular fundus," Vision Res. **36**, 191–205 (1996).
23. G. M. Hale and M. R. Querry, "Optical constants of water in the 200-nm to 200-textmum wavelength region," Appl. Opt. **12**, 555–563 (1973).
24. P. Schiebener, J. Straub, J. M. H. Levelt Sengers, and J. S. Gallagher, "Refractive index of water and steam as function of wavelength, temperature and density," J. Phys. Chem. Ref. Data **19**, 677–717 (1990).
25. E. J. Fernández, A. Unterhuber, P. Prietro, B. Hermann, W. Drexler, and P. Artal, "Ocular aberrations as a function of wavelength in the near infrared measured with a femtosecond laser," Opt. Express **13**, 400–409 (2005).
26. D. A. Atchison and G. Smith, "Chromatic dispersions of the ocular media of human eyes," J. Opt. Soc. Am. A **22**, 29–37 (2005).
27. E. J. Fernández, A. Unterhuber, B. Považay, P. Artal, and W. Drexler, "Chromatic aberration correction of the human eye for retinal imaging in the near infrared," Opt. Express **14**, 6213–6225 (2006).
28. K. Grieve, P. Tiruveedhula, Y. Zhang, and A. Roorda, "Multi-wavelength imaging with the adaptive optics scanning laser ophthalmoscope," Opt. Express **14**, 12230–12242 (2006).
29. E. J. Fernández and P. Artal, "Ocular aberrations up to the infrared range: from 632.8 to 1070 nm," Opt. Express **16**, 21199–21208 (2008).
30. A. Roorda and D. R. Williams, "Optical fiber properties of individual human cones," J. Vision **2**, 404–412 (2002).
31. A. Pallikaris, D. R. Williams, and H. Hofer, "The reflectance of single cones in the living human eye," Invest. Ophthalmol. Vis. Sci. **44**, 4580–4592 (2003).
32. B. Vohnsen, I. Iglesias, and P. Artal, "Guided light and diffraction model of human-eye photoreceptors," J. Opt. Soc. Am. A **22**, 2318–2328 (2005).
33. S. S. Choi, N. Doble, J. Lin, J. Christou, and D. R. Williams, "Effect of wavelength on in vivo images of the human cone mosaic," J. Opt. Soc. Am. A **22**, 2598–2605 (2005).
34. R. S. Jonnal, J. Rha, Y. Zhang, B. Cense, W. Gao, and D. T. Miller, "In vivo functional imaging of human cone photoreceptors," Opt. Express **15**, 16141–16160 (2007).
35. W. Gao, B. Cense, Y. Zhang, R. S. Jonnal, and D. T. Miller, "Measuring retinal contributions to the optical Stiles-Crawford effect with optical coherence tomography," Opt. Express **16**, 6486–6501 (2008).
36. D. T. Miller, L. N. Thibos, and X. Hong, "Requirements for segmented correctors for diffraction-limited performance in the human eye," Opt. Express **13**, 275–289 (2005).
37. American National Standard Institute, *American National Standard for the Safe Use of Lasers ANSI Z* 136.1 – 2000 (American National Standards Institute, New York, 2000).
38. F. C. Delori, R. H. Webb, and D. H. Sliney, "Maximum permissible exposures for ocular safety (ANSI 2000), with emphasis on ophthalmic devices," J. Opt. Soc. Am. A **24**, 1250–1265 (2007).
39. L. Xu, J. Li, T. Cui, A. Hu, G. Fan, R. Zhang, H. Yang, B. Sun, and J. B. Jonas, "Refractive error in urban and rural adult chinese in Beijing," Ophthalmology **112 (10)**, 1676–1683 (2005).

#119325 - $15.00 USD Received 2 Nov 2009; revised 5 Jan 2010; accepted 7 Jan 2010; published 12 Jan 2010

40. A. Sawada, A. Tomidokoro, M. Araie, A. Iwase, T. Yamamoto, and Tajimi study Group, "Refractive errors in an elderly Japanese population: the Tajimi study," Ophthalmology **115 (2)**, 363–370 (2008).
41. J. Schwiegerling, *Field Guide to Visual and Ophthalmic Optics* (SPIE-International Society for Optical Engineering, 2004).
42. E. J. Fernández, L. Vabre, B. Hermann, A. Unterhuber, B. Považay, P. Artal, and W. Drexler, "Adaptive optics with a magnetic deformable mirror: applications in the human eye," Opt. Express **14**, 8900–8917 (2006).
43. N. Devaney, E. Dalimier, T. Farrell, D. Coburn, R. Mackey, D. Mackey, F. Laurent, E. Daly, and C. Dainty, "Correction of ocular and atmospheric wavefronts: a comparison of the performance of various deformable mirrors," J. Opt. Soc. Am. A **24**, 1250–1265 (2007).
44. R. H. Webb and G. W. Hughes, "Scanning Laser Ophthalmoscope," IEEE Trans. Biomed. Eng. **28**(7), 488–492 (1981).
45. R. H. Webb, "Optics for laser rasters," Appl. Opt. **23**, 3680–3683 (1984).
46. Webb, R. H., G. W. Hughes, and F. C. Delori, "Confocal scanning laser ophthalmoscope," Appl. Opt. **26**, 1492–1499 (1987).
47. A. E. Elsner, S. A. Burns, G. W. Hughes, and R. H. Webb, "Reflectometry with a Scanning Laser Ophthalmoscope," Appl. Opt. **31**, 3697–3710 (1992).
48. H. Foroosh, J. B. Zerubia, and M. Berthod, "Extension of phase correlation to subpixel registration," IEEE Trans Image Process **11(3)**, 188–200 (2002).
49. J. C. Wyant and K. Creath, "Basic wavefront aberration theory for optical metrology," in *Applied Optics and Optical Engineering*, Vol. XI, R. R. Shannon and J. C. Wyant, eds. (Academic Press, 1992), 1–53.
50. T. Wilson and A. R. Carlini, "Size of the detector in confocal imaging systems," Opt. Lett. **12**, 227–229 (1987).
51. R. H. Webb, "Confocal optical microscopy," Reports on Progress in Physics **59**(3), 427–471 (1996).
52. Y. Zhang and A. Roorda, "Evaluating the lateral resolution of the adaptive optics scanning laser ophthalmoscope," J. Biomed. Opt. **11(1)**, 014002(1)–014002(5) (2006).
53. C. A. Curcio, K. R. Sloan, Jr., O. Packer, A. E. Hendrickson, and R. E. Kalina, "Distribution of cones in human and monkey retina: individual variability and radial asymmetry," Science **236**, 579–582 (1987).
54. K. Kurokawa, K. Sasaki, S. Makita and Y. Yasuno, "Adaptive optics spectral domain optical coherence tomography with one-micrometer light source," Coherence Domain Optical Methods and Optical Coherence Tomography in Biomedicine XIV, Proc. SPIE, in press.

1. Introduction

Adaptive optics (AO) technology provides high lateral resolution for noninvasive *in vivo* human retinal images by correcting dynamic ocular aberrations. Liang et al. developed an AO flood-illumination system [1], and they successfully improved the image contrast of photoreceptor mosaic. They used a Shack-Hartmann wavefront sensor (SHWS) for measuring ocular aberrations and a deformable mirror to compensate for these ocular aberrations by deforming the shape of the mirror. The AO technology has also been integrated with a confocal scanning laser ophthalmoscopy (AO-SLO) and demonstrated by several groups [2–5]. AO-SLO was used to successfully observe individual photoreceptors, nerve fibers, and the flow of blood cells in retinal capillaries. Because of the confocal property of the AO-SLO, which is the same as that of confocal scanning laser microscopes, it can yield a narrower depth of focus and higher contrast images than a flood-illumination system [6]. Further, it was found that a retinal tracking system and a dual deformable mirror system would further improve the image quality and the stability of the AO-SLO [3, 4, 7]. In a more recent study, AO-optical coherence tomography (AO-OCT) was applied to obtain a three-dimensional microstructured image of the retina, with high isotropic resolution [8–11].

The wavelength-dependent tissue properties affect the retinal image contrast. In some of the recent studies conducted using non-AO-OCT systems, it was shown that the deep region of the eye could be observed with greater clarity using the 1-μm wavelength band than using the standard 840-nm OCT [12–19]. This was because first, 1-μm light is less attenuated by the scattering of the retinal and choroidal tissues and less absorbed by melanin, which exists at the retinal pigment epithelium (RPE) and choroid [18, 20–22]. Second, the local minima in the water absorption spectrum is located at around 1-μm, which is the main content of vitreous. [12, 13, 23, 24].

#119325 - $15.00 USD Received 2 Nov 2009; revised 5 Jan 2010; accepted 7 Jan 2010; published 12 Jan 2010

The chromatic aberration of ocular media also affects the retinal image contrast and image size. Longitudinal and transversal chromatic aberration (LCA and TCA) displace the depth and lateral position of the focus. Hence, it is important to measure and correct chromatic aberration for AO retinal imaging. Within a wavelength range of 400 nm - 900 nm, chromatic aberration of ocular media was well investigated and characterized [25, 26] and most of the AO retinal imaging was demonstrated. In the case of AO-SLO, LCA and TCA between the probe wavelengths were measured by using simultaneous multiwavelength imaging [28]. On the other hand, in the case of AO-OCT, it was found that the use of a broadband light source caused the degradation of image qualities. An achromatizer was used to cancel longitudinal polychromatic aberrations [9, 27]. TCA can be eliminated by aligning the achromatic axis of the eye with the optical axis of the system [9, 28]. At 1-μm wavelength band, ocular aberration was first measured by Fernández et al. using a customized SHWS [29], and it was found that only moderate chromatic aberration existed.

In some studies on vision science, the waveguide property of photoreceptors was investigated using AO retinal imaging systems by employing several approaches [30–35]. It was found that the image contrast of photoreceptors varied only slightly with wavelengths [33]. It is expected that this property is preserved at 1-μm, which may result in high-contrast photoreceptor mosaic images at this wavelength.

In addition, the performance of AO systems depends on the wavelength of light and the pupil diameter. It is known that the required number of actuators decreases with an increase in the wavelength [36]. Long wavelength has high tolerance to the mechanical deformation of mirror surfaces.

On the basis of the above discussions, we concluded that it is worth developing an AO retinal scanner at 1-μm, which is potentially used for SLO and OCT. In this study, we develop an AO retinal scanner, which probes eye aberrations at 840-nm and images the retina at 1.04-μm. This retinal scanner is employed for AO-SLO imaging and used to observe microscopic structures of *in vivo* human retinas.

2. Methods

2.1. Light sources

Two light sources were employed in our AO-SLO; where one source was used for retinal imaging and the other source was used for measuring ocular aberration. The schematic diagram of the proposed system is shown in Fig. 1. An ASE light source (1-Micron ASE source, NP Photonics) with a central wavelength of 1.04-μm and a spectral bandwidth of 62 nm was used for retinal imaging. An 840-nm superluminescent diode (SLD) light source (S840-B-1-20, Superlum) was used as an AO beacon. This shorter wavelength was used for the measurement of the ocular aberration because of the low sensitivity of the CCD of the SHWS at 1-μm.

Before entering the system, beams from the two light sources were coupled using a fiber coupler. The coupling ratio of the fiber coupler was determined on the basis of the output power of the two light sources, optical loss of the system, and the permissible safety limit recommended by the American National Standard Institute (ANSI) [37, 38]. Specifically, the output power of 1-μm ASE light source was 20 mW and that of 840-nm SLD light source was adjustable. The optical loss of the system was approximately 8 dB at 1-μm, which included the optical loss of a beamsplitter placed in front of a fiber collimator. Hence, the splitting ratio of the fiber coupler could be configured to be 80:20, so that the optical powers on the cornea are below the ANSI safety limits It should be noted that the fiber coupler was designed for 1.06-μm and hence, it had relatively high loss at 840-nm. However, the output power of the 840-nm SLD light source was sufficiently high to accept this high optical loss.

The optical powers on the cornea were measured to be 1.1 mW for a 1.04-μm probe and

#119325 - $15.00 USD Received 2 Nov 2009; revised 5 Jan 2010; accepted 7 Jan 2010; published 12 Jan 2010

45 μW for a 840-nm beacon. These optical powers are below the ANSI safety limits [37, 38]. The maximum permissible radiant powers are 1.9 mW at 1.04-μm and 740 μW at 840-nm, respectively, with small spatial extension light sources, the exposure time of > 10 s, and the pupil area of 7 mm. Further, the multiple laser exposure limit was taken into account, i.e., if the optical power of 1.04-μm probe was 1.1 mW, the safety limit power of 840-nm beacon was 300 μW. The optical power of the 1-μm probe beam was configured to be relatively high as compared to that of the conventional 840-nm probe AO-SLO system. This was because of the low responsivity of a Si avalanche photodiode (APD), which detects light backscattered from the retina, and the relatively large water absorption of the ocular media [13].

2.2. Optical design

In order to minimize the size and aberrations of AO retinal scanner, its optical system was carefully designed using an optical computer-aided design system (ZEMAX, ZEMAX Development Corporation, WA). As shown in Fig. 1, for all the relay telescopes except for the Badal optometer placed before the eye pupil, we employed a reflection-type configuration with off-axis relay optics using two spherical mirrors (SMs), as demonstrated as Roorda et. al. [2]. The eye pupil is conjugated to a plane of the lenslet array of the SHWS, a reflective plane of a magnetic deformable mirror (Mirao52d, Imagine Eyes), and horizontal and vertical scanners with $1\times$, $0.3\times$, $1.9\times$, $0.3\times$, and $0.5\times$ magnification, respectively. Cumulative astigmatism originated from the horizontally off-axis SM pairs was canceled by cumulative astigmatism originated from a pair of vertically off-axis SMs (SM5 and SM6) [3]. The pair of vertically off-axis SM relays wavefront from the horizontal scanner to the vertical scanner and vice versa. Further, this optimization process makes the system more compact. The entire system was placed on a compact breadboard with an area of 750×900 mm^2.

We placed a Badal optometer in front of the eye pupil to correct the defocus of the eye, as demonstrated as Burns et. al. [3]. The correctable range was from –9 D to 4 D, which covered more than 99% of the Asian population [39, 40]. In this Badal optometer, the off-axis configuration was used to reduce specular reflection. Refractive powers of the Badal optometer, i.e., both the spherical and the cylinder powers, were calculated from Zernike coefficients [41], as shown in Fig. 2. The magnification from the detection pinhole plane (CP) to the retina was also calculated as a function of the stroke of the Badal optometer, as shown in Fig. 2. These parameters are strongly related to the system design, its performance, and image qualities, as discussed in section 4.2.

In order to investigate the field dependent aberrations of the system, the expected Strehl ratio was calculated over a 2.3 degree field-of-view without sample aberrations and the Badal optometer, as shown in Fig. 3, which contains two-dimensional information. It was greater than 0.95 over a 1.1 degree field-of-view. The field dependent aberrations, such as field curvature and astigmatism degrade the image quality. They depend on deflection angles of scanners and the configuration of off-axis relay telescopes after each scanner. In our system, it was found that the image quality will rapidly degrade along the horizontal direction.

In the mechanical alignment process, the SHWS was used to measure the wavefront at each optically conjugate plane of the pupil, and the optical elements were aligned such that the residual wavefront aberrations of the conjugate planes matched with the numerically predicted aberrations. Cancellation of the cumulative astigmatism was experimentally confirmed, and total residual root-mean-square (RMS) wavefront error of the entire system was found to be less than 0.1 μm.

The specular reflections from the corneal surface and the surfaces of refractive-optics components overlapped the Shack-Hartmann images and reduced the accuracy of wavefront measurement. In order to avoid this problem, two linear polarizers (LP1 and LP2), whose orientations

#119325 - $15.00 USD Received 2 Nov 2009; revised 5 Jan 2010; accepted 7 Jan 2010; published 12 Jan 2010

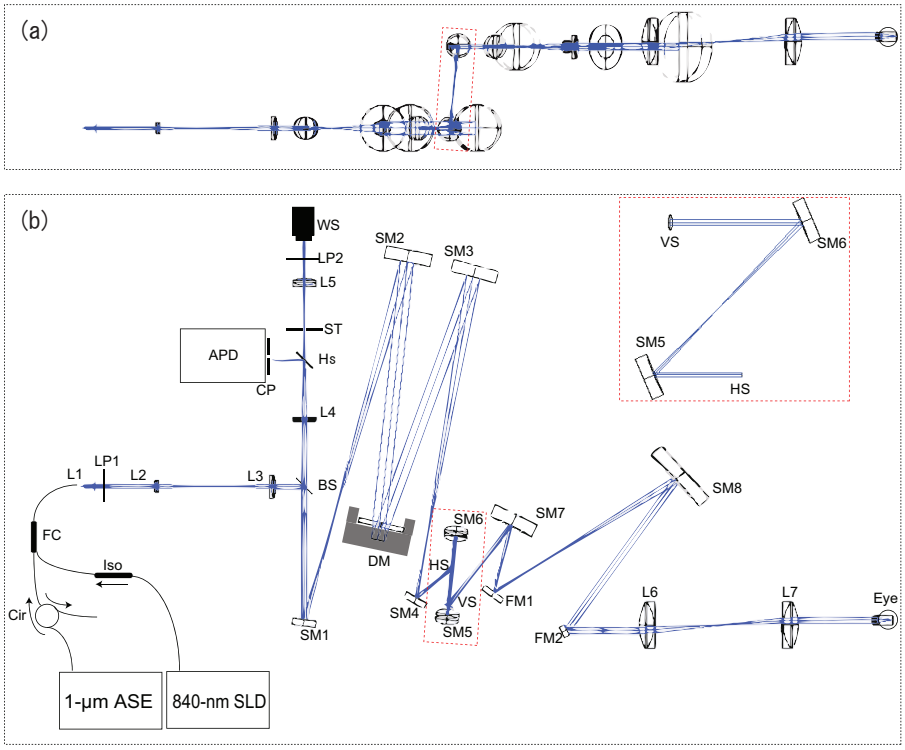

Fig. 1. (a) and (b) are the side and top views of the optical setup of the proposed system, respectively. 840-nm SLD: Superluminescent diode light source, 1-μm ASE: Amplified spontaneous emission light source, FC: Fiber coupler, Cir: Circulator, Iso: Isolator, L#: Achromatic Lenses, LP#: Linear polarizers, BS: Pellicle beam splitter reflects 45% and transmits 55%, CP: Confocal pinhole, ST: Stop, Hs: Harmonic separator reflects 1-μm light and transmits 840-nm light. SM#: Gold-protected spherical mirrors, FM#: Gold-protected flat mirrors, WS: SHWS (Haso32), DM: Deformable mirror (Mirao52d), VS: Vertical scanner, 30 Hz, HS: Horizontal scanner, 15 kHz, APD: Si Avalanche photodiode.

were orthogonal to each other, were placed after L1 and in front of the SHWS, respectively. A stop (ST) blocks the undesired stray light including specular reflection, which is installed in front of L5, as shown in Fig.1.

2.3. Adaptive optics

We used Haso32 (Imagine Eyes, Orsay, France) for the measurement of ocular aberrations. Haso32 is a SHWS, and it comprises a 32 $\times$ 32 lenslet array, where the focal length and size of each lens are 5 mm and 150 μm, respectively [42]. The aperture size of the CCD camera of the SHWS is 3.6 mm $\times$ 3.6 mm, and the unit cell size of the CCD camera is 7.4 μm $\times$ 7.4 μm. The pupil diameter on the SWHS is 2.4 mm, which is limited by the effective aperture of the deformable mirror (Imagine Eyes). Mirao52d (ImagineEyes) is used as a deformable mirror; it is a magnetic deformable mirror with 52 actuators and is employed for the correction of ocular aberrations. The effective aperture of this mirror is 15 mm, and the diameter of the incident beam on it is 13 mm. Mirao52d has a large stroke, tip/tilt wavefront range of –50 - 50 μm peak to valley, and an adequate number of actuators to correct ocular aberrations [42, 43].

#119325 - $15.00 USD Received 2 Nov 2009; revised 5 Jan 2010; accepted 7 Jan 2010; published 12 Jan 2010

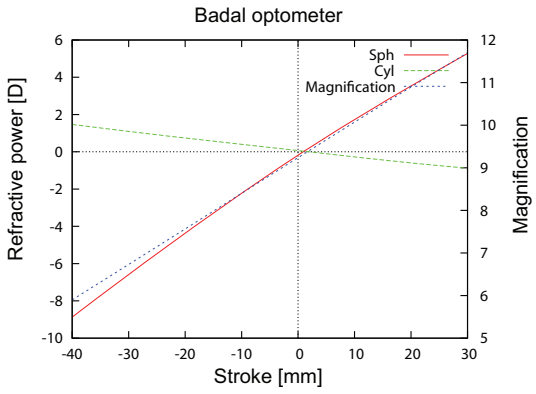

Fig. 2. Refractive powers [D] and magnification.

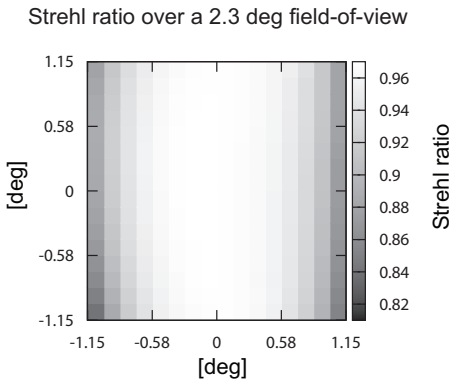

Fig. 3. Strehl ratio calculated over a 2.3 degree field-of-view on the retina.

The SHWS and the deformable mirror form an AO closed loop, which is controlled by an AO software CASAO (ImagineEyes) using a direct slope algorithm. An interaction matrix was obtained by measuring a model eye, which comprises a lens, an iris diaphragm, and a paper target mimicking a refractive-optics of the eye (cornea and crystalline lens), an iris, and a retina. In the measurement, the AO closed loop was configured to have a gain of 0.3. The closed loop was driven at a reputation frequency of 12 Hz.

The difference between the wavelengths of the retinal imaging beam and the wavefront measurement beam caused a difference in the defocus of these beams. The difference between the defocus of the eye at 840-nm and 1-μm was approximately 0.5 D [29]. This difference in the defocus induced a longitudinal focal shift between the imaging and the wavefront measurement beams. However, this focal shift of the imaging beam was eliminated by applying an additional defocus to the target wavefront profile of an AO closed loop. Further, an additional defocus was used to arbitrary shift the focus of the imaging beam along the depth. This arbitrary shift of the focus enables the observation of the selected target layer, such as the photoreceptor layer or the superficial layer of the retina.

The wavefront measurement is synchronized to vertical scan using the frame triggers, in order to avoid the light integration of the CCD camera of the wavefront sensor during the pull-

#119325 - $15.00 USD Received 2 Nov 2009; revised 5 Jan 2010; accepted 7 Jan 2010; published 12 Jan 2010

back action of the slow galvanometric scanner. This synchronization ensures that the pull-back action of the galvanometric scanner does not affect the wavefront measurement.

2.4. Scanning protocol and signal detection

The conventional raster scanning protocol and data acquisition scheme was utilized [44–47]. A 15-kHz resonant scanner (SC30, Electro-Optical Products Corporation, NY) and a 30-Hz galvanometric scanner (6800HP, Cambridge Technology, MA) were used for real-time retinal imaging. The resonant scanner scans the retina along the horizontal direction with a sinusoidal waveform, while, the galvanometric scanner slowly scans the retina along the vertical direction with a sawtooth waveform. The maximum scan angle of the resonant scanner permits a 2.3 degree field-of-view on the retina for the emmetropic eye, which is calibrated using an US Air Force test target (USAF 1951, CVI Melles Griot) that is placed at a retinal conjugated plane in a model eye. For the retinal measurement, the field-of-view was roughly set to be 1.4 degrees. Further calibration of the field-of-view and the location of the measurement was carried out on the basis of the registration of a wide field mosaic image and a color fundus photograph, as described in Section 3.2. In this study, we construct a retinal image only from the forward scan of the resonant scanner, with a frame rate of 15 frames/s.

The backscattered light from the retina is detected by the Si APD (C5331SPL S8890-15, Hamamatsu, Japan) which has higher availability and cost performance than Ge and InGaAs based APD. A confocal pinhole is placed in front of the Si APD. The diameter of the pinhole is 300 μm, which is 10 times the expected radius of an Airy disk projected on the pinhole plane. This relatively large diameter of the pinhole is because of the large optical loss of the ocular media [13] and low responsivity of the Si APD. The output electrical signal is amplified, low-pass filtered with a cut-off frequency of 8 MHz, and digitized with a sampling frequency of 15 MHz using a data acquisition board (NI5122, National Instruments, TX) with a quantum resolution of 14 bits.

2.5. In vivo measurement protocol

Two subjects, i.e., subjects A and B, were involved in *in vivo* imaging. Two drops of 0.5% tropicamide and 0.5% phenylephrine hydrochloride were instilled into the subjects' eyes before performing the measurements, under an appropriate instruction of an ophthalmologist. These instillations were mainly for pupil dilation, although there is an effect of cycloplegia. Prior to AO-SLO imaging, the eyes of the subjects were examined using an auto refractometer (KR-7100P, TOPCON, Tokyo, Japan). The right eye of subject A was found to be highly myopic (Sph: –6.5 D, Cyl: –1.0 D). The left eye of subject B was found to be nearly emmetropic (Sph: –0.6 D, Cyl: –0.5 D). Informed consent was obtained from both the subjects. All the examinations conformed to the declaration of Helsinki, and the protocol was approved by the Institutional Review Board of the University of Tsukuba.

3. Results

3.1. Retinal images

As shown in Figs. 4 (a) and (c), the SLO images did not show any significant contrast when the AO was off and the deformable mirror was flattened. Although most of the defocus was compensated for by the Badal optometer, the small amount of defocus of the eye was fluctuated over the measurement because of the temporal dynamics of ocular aberrations, e.g. unconscious accommodation. The effect of the ocular aberrations appeared as an unintended focal shift and significant signal loss, as shown in Figs. 4 (a) and (c). With AO correction, the image quality and the signal were significantly improved and individual photoreceptors could be observed, as

#119325 - $15.00 USD Received 2 Nov 2009; revised 5 Jan 2010; accepted 7 Jan 2010; published 12 Jan 2010

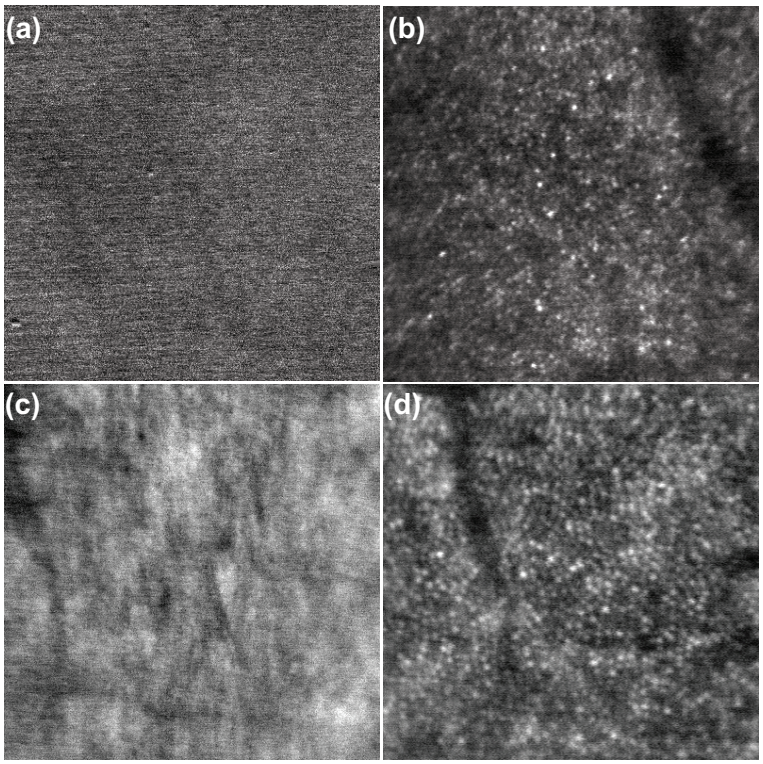

Fig. 4. Subject A examined (a) without AO correction and (b) with AO correction (Media 1). Subject B examined (c) without AO correction and (d) with AO correction (Media 2). Movies of AO-SLO images show the effect of AO correction, and these high-quality versions are available (Media 3 and Media 4). Field-of-view of these cropped images was 1 degree $\times$ 1 degree for the emmetropic eye.

shown in Figs. 4 (c) and (d). The signal to noise ratio and the lateral resolution were improved. Figs. 4 (a) and (b) were obtained from subject B at an eccentricity of 5 degree nasal. Figs. 6 (c) and (d) were obtained from subject B at an eccentricity of 6 degree nasal. Although white dots appeared in (Media 1) were the artifacts caused by dusts, they have sufficiently smaller signals compared to the signals with AO.

The residual RMS wavefront error was less than 0.1 μm and was typically around 0.06 μm for both cases. This RMS wavefront error implies that the Strehl ratio is greater than 0.69 and typically 0.88. Corresponding lateral resolution was greater than 4 μm and typically 3.4 μm. More details about the estimation of lateral resolution is described in Section 4.2.

Movies of the AO-SLO images show the effect of AO-correction ((Media 1) and (Media 2)). In the movies, a subpixel phase-correlation-based registration is applied to eliminate the eye movement [48].

3.2. Calibration of the eccentricity

Eccentricity was calibrated by manual image registration. Figure 5 shows a wide-field retinal image montage, which is registered with a fundus photograph. The blood vessels were used as a reference feature for registration. The yellow circles/arcs represent the eccentricity contours, which were obtained from the parameters of the fundus camera.

#119325 - $15.00 USD Received 2 Nov 2009; revised 5 Jan 2010; accepted 7 Jan 2010; published 12 Jan 2010

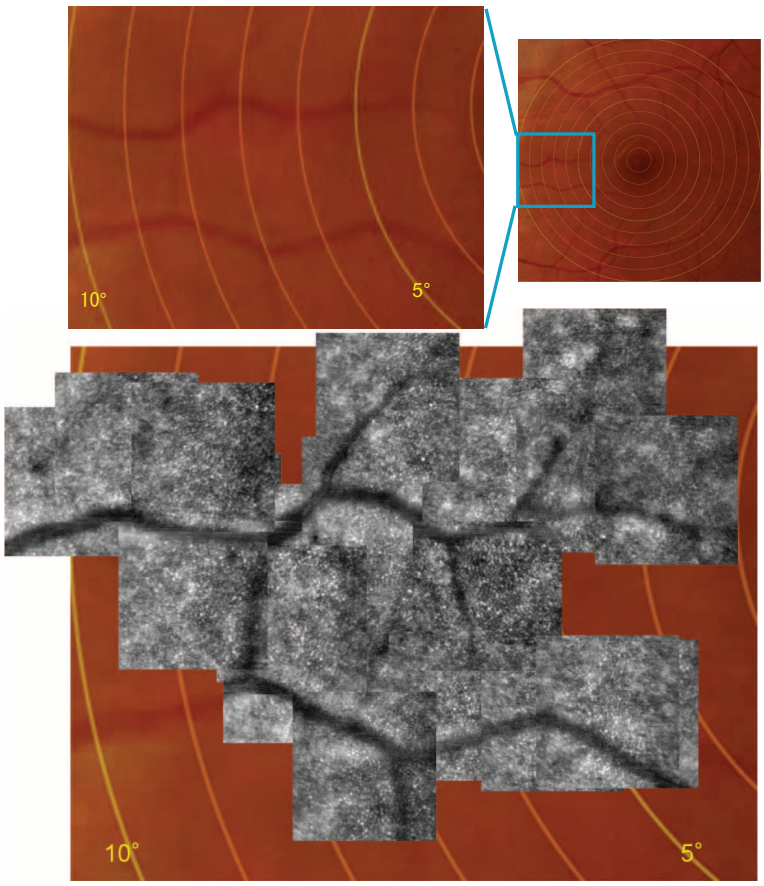

Fig. 5. Wide-field retinal image montage obtained by manual registration of several images. Yellow circles/arc represent the eccentricity contours.

3.3. *Effect of additional defocus*

In order to observe the effect of additional defocus, the focus was shifted along the depth by applying an additional defocus (Z_2^0 = 1.0 μm) to the target wavefront during the AO-SLO measurement of the left eye of subject B at 5 degree eccentricity at superior. Figure 6 (a) and (Media 5) show the retinal image without additional defocus. The focus is on the photoreceptor layer, and the photoreceptor mosaic is visible. Figure 6 (b) and (Media 6) show the retinal image with a defocus of 1.0 μm. The focus is shifted to the retinal surface, and the flowing blood cells in the retinal blood vessels are observed.

4. Discussion

4.1. *AO retinal imaging with one-micrometer light source*

The long wavelength provides a low transform-limited lateral resolution, which is a disadvantage of the 1-μm wavelength AO retinal imaging. The typical transversal resolution shown in this study was 3.4 μm.

However it is easier to achieve diffraction limited resolution with a longer wavelength than a shorter wavelength. This is because the Strehl ratio *Sr* can be represented by the following

#119325 - $15.00 USD Received 2 Nov 2009; revised 5 Jan 2010; accepted 7 Jan 2010; published 12 Jan 2010

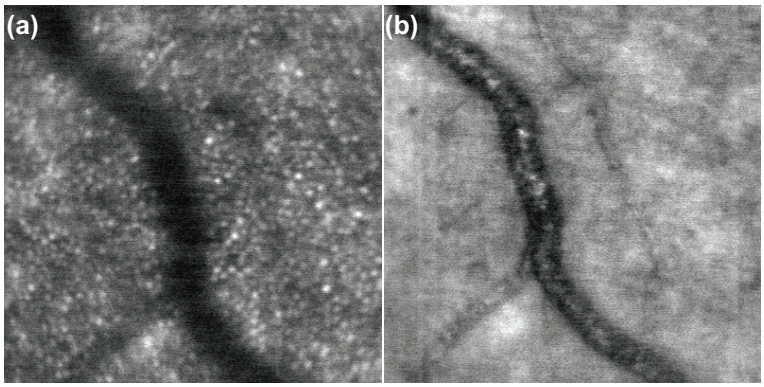

Fig. 6. AO-SLO image with focal shift at retina. (a) Incident beam focused on the photoreceptor layer (Media 5). (b) Incident beam focused on the inner retinal layer (Media 6). Movies of the AO-SLO images show the effect of the additional defocus, and these high-quality version are available (Media 7) and (Media 8)).

approximation [49]:

$$Sr \approx \exp\left\{-\left(\frac{2\pi\delta}{\lambda}\right)^2\right\} \tag{1}$$

Where δ is the residual RMS wavefront error, and λ is the wavelength of light. According to the Maréchal criterion, the abovementioned approximation is valid only for Sr $\geq$ 0.1. An optical system with $Sr > 0.8$ is regarded as a transform-limited system.

This indicates that the AO retinal imaging with 1-μm light makes easy to stably achieve high resolution in practical situation in whtich the measurement was disturbed by dynamic aberrations and mechanical vibrations.

4.2. Estimation of lateral resolution

Lateral resolution of the 1-μm wavelength AO-SLO was estimated from the full width at half maximum of the point spread function (*PSF*) by taking into account aberrations.

In confocal microscopy, the *PSF* is represented by the following equation [50, 51]:

$$PSF = PSF_{ill} \times (PSF_{obs} * D) \tag{2}$$

here PSF_{ill} and PSF_{obs} are point spread functions of illumination and observation, respectively. D is the pupil function of the detection pinhole, whose diameter, d, is corrected by the magnification from the pinhole plane to the retinal plane as $d = M \times a$, where M is the magnification, and a is the physical diameter of the pinhole. Here, M and a are 9.3 and 300 μm, respectively; they have been to estimate the lateral resolution of the 1-μm wavelength AO-SLO (see Section 3.1). It should be noted that M = 9.3 is only valid for the emmetropic eye because it depends on the stroke of the Badal optometer (see Section 2.2).

Although the similar analysis was performed by several researchers [50–52], they did not take into account the deformation of *PSF* casued by aberrations precisely with confocal effect.

#119325 - $15.00 USD Received 2 Nov 2009; revised 5 Jan 2010; accepted 7 Jan 2010; published 12 Jan 2010

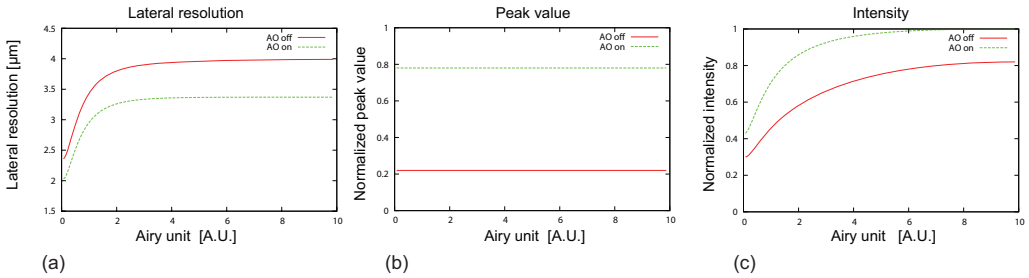

Fig. 7. (a) Lateral resolution, (b) maximum peak value of *PSF*, and (c) normalized intensity of *PSF*, which is calculated from the double integral of *PSF*. Horizontal-axis corresponds to the physical diameter of the pinhole in Airy unit [A.U.].

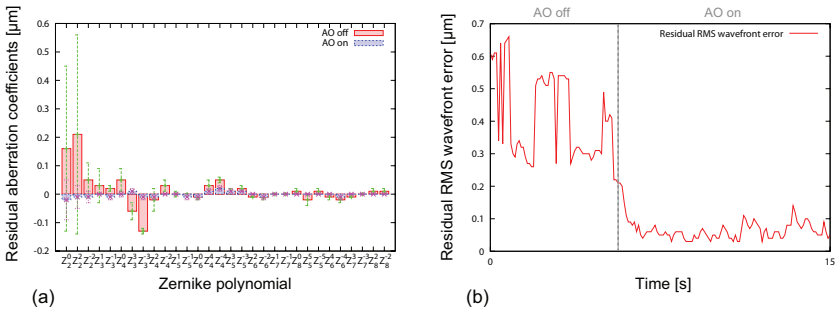

Fig. 8. (a) Residual aberration coefficients and (b) residual RMS wavefront error, which are measured using the SHWS (Haso32). The error bars (green and red) in (a) represent the standard deviation of the residual aberration coefficients of AO-off and AO-on, respectively.

We defined PSF_{ill} and PSF_{obs} as

$$\begin{aligned} PSF_{ill}(X,Y) &= c\left|\mathscr{F}\left\{I(x,y)\exp\left(\frac{-2\pi i(W(x,y)+w_{ill}(x,y))}{\lambda}\right)\right\}\right|^2 \\ PSF_{obs}(X,Y) &= c\left|\mathscr{F}\left\{I(x,y)\exp\left(\frac{-2\pi i(W(x,y)+w_{obs}(x,y))}{\lambda}\right)\right\}\right|^2 \end{aligned} \tag{3}$$

Where, X,Y are the positions on the retinal image plane, x,y are the positions on the pupil plane, $I(x,y)$ represents the intensity profiles on the pupil plane, $W(x,y)$ represents the ocular aberrations, w_{ill} and w_{obs} are the system aberrations of the illumination and observation path, respectively, λ is the wavelength of the probe light, and c is the proportionality coefficient. For simplicity, because the difference between w_{ill} and w_{obs} is sufficiently smaller than $W(x,y)$, we assumed that PSF_{ill} is approximately equal to PSF_{obs}.

We used Eqs. (2) and (3) to estimate the lateral resolution, maximum peak value, and the double integral of *PSF* as a function of the diameter of the pinhole, as shown in Fig. 7. The curves of AO-on and AO-off were calculated on the basis of typical aberrations of a normal subject measured using our AO retinal scanner while AO was turned on and turned off, respectively. The residual amount of the aberration coefficients and that of the RMS wavefront error are shown in Figs. 8 (a) and (b), respectively.

The diameter of the photoreceptor cell increases from 2 μm with an increase in the eccentricity [53]. The same trend can be observed in the case of photoreceptor spacing. In the 1-μm

#119325 - $15.00 USD Received 2 Nov 2009; revised 5 Jan 2010; accepted 7 Jan 2010; published 12 Jan 2010

wavelength AO-SLO, the Airy disk radius on the retina is 3.3 μm, and it is difficult to resolve the small photoreceptor at an eccentricity of 0 degree. In order to resolve this, a sufficiently small value of d is required, as shown in Fig. 7 (a). However, such a value of d causes significant optical loss by pinhole rejection, as shown in Fig. 7 (c). In the typical AO-SLO, d is typically 3 - 10 times that of the Airy disk radius [3, 28] to maximize the collection ratio of the back-scattered photon.

On the other hand, OCT was an interference detection scheme and hence has higher sensitivity than SLO. In reality, most of the OCT systems typically use a single mode fiber, which provides higher confocal effect than that of typical AO-SLO.

5. Conclusion

In spite of the disadvantage of the relatively low transform-limited resolution at longer wavelengths, the 1-μm wavelength AO-SLO was successfully used to observe individual photoreceptors. Different depths of the retina were distinctly observed using different values of additional defocus. Further the AO retinal scanner has potentially capable of combining with OCT system. In fact, a preliminary demonstration of 1-μm wavelength AO-OCT was started [54]. The AO retinal scanner for 1-μm wavelength would provide high penetration and high resolution microstructural information of the retina.

Acknowledgment

This research was supported in part by Japan Science and Technology Agency.

#119325 - $15.00 USD Received 2 Nov 2009; revised 5 Jan 2010; accepted 7 Jan 2010; published 12 Jan 2010